Published in final edited form as:
Acta Neuropathol. 2013 February ; 125(2): 187–199. doi:10.1007/s00401-012-1065-6.

PRESENILIN-1 ADOPTS PATHOGENIC CONFORMATION IN NORMAL AGING AND IN SPORADIC ALZHEIMER'S DISEASE

Lara Wahlster[1,2,*], **Muriel Arimon**[1,*], **Navine Nasser-Ghodsi**[1], **Kathryn Leigh Post**[1], **Alberto Serrano-Pozo**[1], **Kengo Uemura**[1], and **Oksana Berezovska**[1,†]

[1]MassGeneral Institute for Neurodegenerative Disease, department of Neurology, Massachusetts General Hospital, Harvard Medical School, CNY 114, 16th Street, Charlestown 02129, Massachusetts, USA

[2]Institute of Physiology and Pathophysiology, University of Heidelberg, INF 326, 69120 Heidelberg, Germany

Abstract

Accumulation of amyloid-β (Aβ) and neurofibrillary tangles in the brain, inflammation and synaptic and neuronal loss are some of the major neuropathological hallmarks of Alzheimer's disease (AD). While genetic mutations in amyloid precursor protein and presenilin-1 and -2 (PS1 and PS2) genes cause early-onset familial AD, the etiology of sporadic AD is not fully understood. Our current study shows that changes in conformation of endogenous wild type PS1, similar to those found with mutant PS1, occur in sporadic AD brain and during normal aging. Using a mouse model of Alzheimer's disease (Tg2576) that overexpresses the Swedish mutation of amyloid precursor protein but has normal levels of endogenous wild-type presenilin, we report that the percentage of PS1 in a pathogenic conformation increases with age. Importantly, we found that this PS1 conformational shift is associated with amyloid pathology and precedes amyloid-β deposition in the brain. Furthermore, we found that oxidative stress, a common stress characteristic of aging and AD, causes pathogenic PS1 conformational change in neurons *in vitro,* which is accompanied by increased A 42/40 ratio. The results of this study provide important information about the timeline of pathogenic changes in PS1 conformation during aging, and

†To whom correspondence should be addressed: Oksana Berezovska, Ph.D., Associate Professor, MassGeneral Institute for Neurodegenerative Disease (MIND), Massachusetts General Hospital, Harvard Medical School, 114 16th Street, Charlestown, MA 02219, USA, Phone: 617-726-7478, Fax: 617-724-1480, OBerezovska@partners.org.
*Both authors contributed equally to this work
1. First Name: Lara Last Name: Wahlster
MassGeneral Institute for Neurodegenerative Disease, Department of Neurology, Massachusetts General Hospital, Harvard Medical School, Address: 114 16th Street, Charlestown, MA 02129, USA, wahlster@stud.uni-heidelberg.de
2. First Name: Muriel Last Name: Arimon
MassGeneral Institute for Neurodegenerative Disease, Department of Neurology, Massachusetts General Hospital, Harvard Medical School, Address: 114 16th Street, Charlestown, MA 02129, USA, Arimon.Muriel@mgh.harvard.edu
3. First Name: Navine Last Name: Nasser-Ghodsi
MassGeneral Institute for Neurodegenerative Disease, Department of Neurology, Massachusetts General Hospital, Harvard Medical School, Address: 114 16th Street, Charlestown, MA 02129, USA, NNasserghodsi@gmail.com
4. First Name: Kathryn Leigh Last Name: Post
MassGeneral Institute for Neurodegenerative Disease, Department of Neurology, Massachusetts General Hospital, Harvard Medical School, Address: 3114 16th Street, Charlestown, MA 02129, USA, klpost@partners.org
5. First Name: Alberto Last Name: Serrano-Pozo
MassGeneral Institute for Neurodegenerative Disease, Department of Neurology, Massachusetts General Hospital, Harvard Medical School, Address: 114 16th Street, Charlestown, MA 02129, USA, ASerrano1@partners.org
6. First Name: Kengo Last Name: Uemura
MassGeneral Institute for Neurodegenerative Disease, Department of Neurology, Massachusetts General Hospital, Harvard Medical School, Address: 114 16th Street, Charlestown, MA 02129, USA, ueken@kuhp.kyoto-u.ac.jp
7. First Name: Oksana Last Name: Berezovska
MassGeneral Institute for Neurodegenerative Disease, Department of Neurology, Massachusetts General Hospital, Harvard Medical School, Address: 114 16th Street, Charlestown, MA 02129, USA, OBerezovska@partners.org

suggest that structural changes in PS1/-secretase may represent a molecular mechanism by which oxidative stress triggers amyloid-β accumulation in aging and in sporadic AD brain.

Keywords

Alzheimer's disease; aging; presenilin-1; amyloid beta; oxidative stress

INTRODUCTION

Alzheimer's disease (AD) is characterized by deposition of senile plaques composed of amyloid-(A) peptide, accumulation of tau-containing neurofibrillary tangles, and synaptic and neuronal loss. Numerous biochemical and genetic studies point to A as an essential trigger for the disease [24], even though neuropathological features such as neurofibrillary tangles, synaptic loss and neuronal loss show better correlation with dementia progression and severity of the disease [19,20,64,15]. It has been proposed that the longer and more aggregation-prone A species, such as Aβ 42 or Aβ 43, are implicated in neurotoxicity linked to AD [11,55]. Strong evidence has been presented that the ratio of the Aβ42 to Aβ40 peptides, rather than absolute Aβ levels, plays a crucial role in neurodegeneration [71,41,70,5,37]. Importantly, A plaques have been previously observed post-mortem in cognitively normal elderly individuals [2], and more recent A imaging studies consistently report that ~20–30% of individuals with no clinical signs of dementia show significant A deposition in the brain [29,54]. These findings indicate that amyloid pathology precedes the cognitive decline that defines AD dementia, and thus may be the trigger of a cascade of events that leads to neuronal structural and functional abnormalities, and ultimately to age-related memory impairment [26].

Aβ peptides of various lengths are generated after sequential cleavage of the amyloid precursor protein (APP) by - and γ-secretases [reviewed in 60,14]. The catalytic subunit of the -secretase enzyme complex is a 467 amino acid protein with nine-transmembrane domains named presenilin-1 (PS1) [72,13]. Topological studies suggest that PS1 adopts an intramembranous ring-like structure, with N- (NT) and C-termini (CT) in close proximity, which is critical for its function [1]. PS1 holoprotein is inactive and only becomes mature and catalytically active after undergoing an endoproteolytic cleavage [66]. More than 160 mutations have been identified that are located throughout the entire sequence of the PS1 molecule and are associated with early-onset familial AD (fAD) [Alzheimer Disease & Frontotemporal Dementia Mutation Database: http://www.molgen.ua.ac.be/ADMutations10]. We have previously shown that fAD-linked mutations in PS1 lead to a consistent change in PS1 conformation, alter APP positioning within the membrane, and affect PS1/-secretase alignment with the APP substrate [4,67]. Using a variety of genetic and pharmacological manipulations, others and we have established that changes in conformation of PS1 are associated with shifts in the A 42/40 ratio [28,4,42,61]. These conformational changes are very subtle and transitory, and may be overlooked by conventional biochemical methods. For this reason, we employ high spatial resolution Fluorescence Lifetime Imaging Microscopy (FLIM) technique to detect relative changes in the proximity between N- and C-termini of endogenous PS1 in its normal physiological environment in intact neurons in fixed brain sections. We have previously established that "closed" PS1 conformation (i.e. more compact structure, shorter PS1 NT-CT distance by FLIM) correlates with predominant cleavage of APP at ≥A 42 position and therefore with an increase in the Aβ42/40 ratio. Conversely, an "open" PS1 conformation (larger PS1 NT-CT distance) is associated with predominant cleavage at ≤A 40 and a decrease in the Aβ42/40 ratio [4,68,42]. Thereby, PS1 conformation sensitive FLIM assay can be used as an indirect but reliable readout for changes in the Aβ42/40 ratio *in vitro* and *in vivo*.

An increase in the A 42/total ratio was observed in sAD patients, compared to that in age-matched normal controls [27,41]. It has been also proposed that levels of A 43 rather than A 42 change progressively in sporadic MCI/AD patients [32]. Furthermore, a small but significant increase in the A 42/40 ratio has been shown to occur during normal aging in the wild type mouse brain [52,73].

Although a direct relationship between mutations in PS1, changes in APP processing/A generation, and development of fAD has been established, the etiology of sporadic AD (sAD), which represents the vast majority of AD cases, is not fully understood. In addition, although aging is the main risk factor for developing sAD, the critical link between "normal" aging and the disease remains unclear.

In this work we present data supporting the hypothesis that in sAD and during normal aging the conformation of wild type PS1 shifts towards a "closed" PS1 conformation, similar to that found in PS1 with fAD-causative mutations [4]. By employing the FLIM assay in brain tissue sections we present evidence for a significant increase of the proportion of neurons with "closed" PS1 conformation in sAD cases, compared to cognitively normal age-matched controls. We also show that PS1 conformational changes are more pronounced in neurons close to A plaques. This pathogenic change in PS1 seems to precede plaque deposition in the Tg2576 mouse model of AD. Importantly, we found that the observed phenomenon also occurs in wild-type mice as they age. Finally, we demonstrate that oxidative stress can be a triggering factor which induces a pathogenic "closed" conformational state of endogenous wild type PS1 in neurons *in vitro* and increases the A 42/40 ratio.

MATERIAL & METHODS

Human tissue

Brain tissue of non-demented control subjects (n=10, mean age± SD 92.0 ± 9.9 years), sporadic AD patients (n=10, mean age± SD 86.6 ± 10.5 years), and frontotemporal lobar degeneration (FTLD) patients (n=5, mean age± SD 77.7 ± 8.9 years) was obtained from the brain bank of the Alzheimer Disease Research Center at Massachusetts General Hospital (Supplementary Table 1). Control cases were non-demented individuals who did not meet pathological diagnostic criteria of AD or any other neurodegenerative disease at autopsy. All AD cases met clinical and pathological diagnostic criteria of AD [51,46]. FTLD patients were diagnosed according to published criteria [47,31,44]. Both AD and FTLD patients and non-demented control individuals were matched by post-mortem interval (PMI). AD patients and controls were also matched by age whereas, as expected from its typically earlier onset, patients with FTLD were significantly younger (Kruskal-Wallis ANOVA: $p=0.0271$; Dunn's Multiple Comparison Test CTRL vs AD: n.s.; CTRL vs FTLD: $p<0.05$) (Supplementary Table 1). Based on the power analysis, it is possible to detect a moderate effect (lifetime difference) with 90% power using 8–10 human cases, assuming a 10–15% SD in measurements and an effect size of one SD. Five to eight brain sections from each brain were used for the FLIM assay. For immunohistochemical analysis, medial temporal lobe specimens fixed in paraformaldehyde (PFA) at 4°C for at least 48 hours were used. Coronal sections (50 μm) of the hippocampus were obtained using a freezing microtome (Leica SM 2000R, Bannockburn, IL).

Mouse tissue

Tg2576 transgenic mice expressing the Swedish mutant of human APP (K670N/M671L huAPP695) [25], and non-transgenic littermates (background strain C57-B6) (Charles River Laboratories, Wilmington, MA) were used. Mice were divided into three age groups: "*young*" animals (1–4 months), "*adults*" (7–9 months) and "*old*" animals (17–25 months); each age group included three transgenic and three control mice.

For all experiments transgenic animals were compared to non-transgenic littermates. Data from female and male mice were combined after confirming no sex-related differences in PS1 conformation. Mice were kept in a light-dark cycle, temperature and humidity controlled animal facility with *ad libitum* food and water. All animal experiments were approved by the Subcommittee for Research Animal Care at Massachusetts General Hospital.

Mice were euthanized with CO_2 and immediately perfused using PBS and 4% PFA. Brains were removed and fixed by immersion in 4% PFA containing 15% glycerol cryoprotectant for at least 48 hours at 4°C. Brains were then sectioned on a Leica freezing microtome (Leica SM 2000R, Bannockburn, IL) at 35-μm thickness, and the resulting free-floating sections were stored at −20°C in Tris-buffer solution (TBS) (Fisher Scientific, Waltham, MA) with 15% glycerol (Sigma-Aldrich, St. Louis, MO) until used.

Primary neuronal cultures

Primary neuronal cultures were obtained from cerebral cortex of mouse embryos at gestation day 14–16 (Charles River Laboratories, Wilmington, MA), as described previously [3]. Briefly, the dissected tissue was dissociated by trypsinization for 5 minutes and re-suspended in neurobasal medium (Gibco, Invitrogen, Gaithersburg, MD) supplemented with 10% fetal bovine serum (Gibco, Invitrogen), 2 mM/L L-glutamine (Gibco, Invitrogen), 100 U/mL penicillin and 100 μg/mL streptomycin (Gibco, Invitrogen). Neurons were seeded to a density of 4.5×10^5 viable cells in 35-mm glass bottom culture dishes (MatTek Corporation, Ashland, MA) previously coated with Poly-D-lysine hydrobromide at 100 μg/ml (Sigma-Aldrich, St. Louis, MO). Cultures were maintained at 37 °C with 5% CO_2 in neurobasal medium supplemented with 2% B27 nutrient (Gibco, Invitrogen), 2 mM L-glutamine, penicillin and streptomycin. Neurons at 5–11 days *in vitro* were treated as described in the following section, and subsequently immunostained for the FLIM analysis.

In vitro drug treatment

To induce oxidative stress, primary neurons were treated with either 100 μM 4,4′-dithiodipyridine (DTDP) (Sigma-Aldrich) or 1 mM 4-hydroxynonenal (HNE) (Cayman Chemical, Ann Arbor, MI) (both diluted in ethanol) for 20 min. In parallel experiments, the antioxidant N-acetylcysteine amide (NACA) (Sigma-Aldrich) (diluted in DMSO), was used at 750 μM for 16 hours prior to adding oxidative agents. Neuronal viability and potential toxicity due to the treatment was assessed by visual inspection of neuronal morphology and by monitoring the release of Adenylate Kinase in the culture medium using the ToxiLight Bio Assay kit (Cambrex, Rockland, ME). To assess PS1 conformation by FLIM, cells were either transfected with the GFP-PS1-RFP FRET reporter probe [68] before the treatment and analysis, or fixed and subjected to immunocytochemistry-based FLIM as described below.

A quantification

The conditioned media was collected from primary neurons treated with DTDP or HNE (or vehicle control) for 3h, and both A 40 and A 42 were quantified by ELISA (Human/Rat Amyloid (40 or 42) ELISA Kits, Wako, Japan). The capture antibody was BNT77 and the detection antibody was HRP-conjugated BA27 for Aβ 40 and BC05 for Aβ 42, all of which recognize mouse Aβ.

Immunohistochemistry and immunocytochemistry

PFA fixed primary neurons, and human and mouse free-floating tissue sections were washed with TBS and permeabilized in blocking buffer (2.5% skimmed milk, 1.5% Normal Donkey Serum, 0.1% Triton-X100 in TBS) for 60 minutes. Samples were then incubated overnight

at 4°C with the respective primary antibodies (goat-PS1-NTF, 14–33 aa, Millipore, Billerica, MA; and rabbit-PS1-CTF, 450–467 aa, Sigma-Aldrich) in blocking buffer. Alexa488- and Cy3-conjugated secondary antibodies (donkey-anti-goat AlexaFluor488, Invitrogen; and donkey-anti-rabbit Cy3, Jackson ImmunoResearch, West Grove, PA) were used for detection. Sections were coverslipped with Vectashield mounting medium (Vector Laboratories, Burlingame, CA), sealed, and stored at 4°C until imaging. To identify Aβ plaques in tissue sections, coverslips were removed from slides after image acquisition, and the sections were incubated in a solution of 0.05% Thioflavin S (ThioS) (Sigma, St. Louis, MO) (in 50% ethanol) for 5 min and differentiated with 80% ethanol (2 × 30 seconds). Sections were again coverslipped as described above. Previously imaged neurons were stereotactically located using the XY coordinate system on the motorized stage of a Zeiss LSM 510 microscope (Carl Zeiss Inc., Oberkochen, Germany) and their distance to the closest ThioS positive A plaque was measured.

Fluorescence Lifetime Imaging Microscopy (FLIM)

The conformation of PS1 molecules (relative proximity between fluorescently labeled PS1 NT and CT) was monitored using Fluorescence Lifetime Imaging microscopy (FLIM), a Förster Resonance Energy Transfer (FRET)-based technique, as previously described [4,42]. FRET occurs when two fluorophores with overlapping emission and excitation spectra are in close proximity to each other (<5 nm), causing a decrease in the donor fluorophore lifetime due to a partial non-radiative transfer of its emission energy to the acceptor fluorophore [39]. We measured fluorescence lifetime rather than intensity because lifetime is an intrinsic biophysical property of fluorophores and, unlike fluorescence intensity, does not depend on the concentration or stoichiometry of the donor and acceptor fluorophores [39,38]. Multi-exponential analysis of the donor fluorophore lifetimes was performed using Becker&Hickl FLIM software to distinguish between PS1 molecules in different conformational states. We used two-component analysis for cells *in vitro* as described in details previously [4,42,68]. For brain tissue samples we used three-component analysis of the fluorescence lifetimes to account for presence of autofluorescence (Jones et al., 2008). Briefly, mouse and human brain sections were immunostained using Alexa488 as the donor fluorophore to label PS1 NT and Cy3 as the acceptor fluorophore to label PS1 CT (see above). A Chameleon Ti:Sapphire laser (Coherent Inc., Santa Clara, CA) was used to excite the donor fluorophore (two-photon excitation at 780 nm wavelength). Donor fluorophore lifetimes were recorded using a high-speed photomultiplier tube (MCP R3809; Hamamatsu, Bridgewater, NJ) and a fast time-correlated single-photon counting acquisition board (SPC-830; Becker & Hickl, Berlin, Germany). FLIM data analysis was performed using SPC Image (Becker & Hickl, Berlin, Germany), and interference of the endogenous tissue auto-fluorescence (AF) with the analysis was eliminated based on techniques described by Jones et al. [30]. Briefly, first, the lifetime of tissue auto-fluorescence (t1) was determined in tissue sections prior to immunostaining. For the donor fluorophore lifetime measurements, each neuron was outlined and average lifetime per cell was measured by fitting raw data to a multi-exponential decay curve. To establish the baseline Alexa-488 donor fluorophore lifetime in the absence of the Cy3-acceptor (t2, negative control), and to exclude the interference of the AF with the FLIM analysis, a double-exponential fit was performed in which t1= AF lifetime was fixed and removed from the analysis, and the t2= donor lifetime was recorded. To measure the donor fluorophore lifetime shortening in the presence of the Cy3 acceptor fluorophore, the lifetimes for each tissue specimen were fitted to three fluorescence decay curves. For this, t1= AF and t2= donor lifetime in the absence of FRET were fixed and removed from the analysis, while t3= shortened donor lifetime due to FRET was recorded and used for statistical analyses.

Thus, FRET efficiency ($\%E_{FRET}$) was calculated as the percent of decrease in the lifetime of the A488 donor fluorophore due to the presence of the Cy3-acceptor fluorophore using the following equation:

$$\%E_{FRET} = 100^{*}(t2-t3)/t2,$$

where t2 is the lifetime of the A488 donor fluorophore alone (FRET absent), and t3 is the A488 lifetime in the presence of Cy3 (FRET present). $\%E_{FRET}$ rises as the donor to acceptor fluorophore proximity increases ("closed" PS1 conformation), whereas lower $\%E_{FRET}$ reflects an increased donor-to-acceptor distance ("open" PS1 conformation). A 128×128 pixel matrix was created to display lifetimes on a pixel-by-pixel basis in pseudocolored images. Green-to-red pixels represent shorter lifetimes (FRET present), whereas blue pixels represent longer lifetimes (FRET absent).

Of note, our FLIM assay only monitors changes in conformation of the PS1 molecules assembled into active -secretase complexes, since inactive PS1 holoprotein does not support FRET [4]. Thus, the multi-component FLIM analysis allows to distinguish these two populations: inactive PS1 (no FRET, excluded from the analysis), and active PS1 (FRET present, although with different degrees of FRET efficiency values that reflect different PS1 conformations).

Statistical analysis

Statistical analysis was performed using Graph Pad Prism 4 software (GraphPad Software Inc., La Jolla, CA). Data is expressed as mean ± SD or mean ± SEM, as stated in the figure legends. Two-sided Student's t-test and ANOVA with Bonferroni's post-hoc correction were used for 2-group and 3-group comparisons, respectively. D'Agostino & Pearson omnibus normality test was used to evaluate the normality of the distributions of $\%E_{FRET}$ values. In addition, to investigate whether the $\%E_{FRET}$ values fit into a bimodal distribution, a Goodness-of-fit-test (null hypothesis: simple Gaussian versus alternative hypothesis: sum of 2 Gaussians) was used. Values were considered significant at $p<0.05$ (*). Higher significance is indicated as follows: ** $p<0.01$, *** $p<0.001$.

RESULTS

Familial-AD-like PS1 conformational changes occur in sporadic Alzheimer's disease

To determine if PS1 conformational changes characteristic of fAD mutants [4] occur in the brain of sAD patients, we evaluated PS1 conformation in CA1 hippocampal pyramidal neurons in brain sections of sAD patients. For this, relative proximity between the PS1 N- and C-termini was monitored by calculating the FRET efficiency ($\%E_{FRET}$) in immunohistochemistry-based FLIM assay (see Materials and Methods).

We found that average $\%E_{FRET}$ was significantly higher in hippocampal neurons of sAD patients (13.4 ± 4.7%), compared to that in controls (9.0 ± 2.7%) (Fig. 1a), indicating shorter distance between the PS1 NT-CT, i.e. an overall more "closed" PS1 conformation in the former. To investigate whether this change is specific to AD, we performed immunohistochemistry-based FLIM on brain sections from frontotemporal lobar degeneration (FTLD) patients. Remarkably, the average $\%E_{FRET}$ value in hippocampal neurons of FTLD patients (8.7 ± 2.1%) was comparable to that of the control group, suggesting a specific link between PS1 conformational changes and AD-related pathology (Fig. 1a).

Interestingly, $\%E_{FRET}$ values in sporadic AD patients showed a double Gaussian distribution according to Goodness-of-fit test (mean1 = 12.1 ± 4.1%, mean2 = 22.3 ± 1.6%) (Fig. 1b), revealing of a distinct subpopulation of neurons with even more "closed" PS1 conformation Noteworthy, a double Gaussian distribution was also observed for the $\%E_{FRET}$ values for age-matched controls, with a small subpopulation of neurons also displaying predominantly "closed", pathogenic PS1 conformation in the brain of non-demented individuals (mean1 = 8.3 ± 2.3%, mean2 = 15.8 ± 0.7%) (Fig.1b). The presence of these two populations in both control and AD groups suggest that either these neurons are more susceptible to PS1 conformational changes or that they are exposed to some local insult capable of changing PS1 conformation.

PS1 conformation correlates with proximity to A plaques

To investigate whether the subpopulation of neurons with "closed" PS1 conformation (high $\%E_{FRET}$) in sporadic AD were associated with A plaques, the coverslips were removed and the same sections were counterstained with ThioS to visualize A plaques. The CA1 region of hippocampus was selected for the analysis because it has a relatively low density of plaques compared to the other brain regions [7], hence decreasing the chance of having a plaque in an adjacent section. The density of ThioS positive dense core plaques (DCP) in the CA1 area of the patients used in the study was 4.4 ± 2.8 DCP/mm^2 (mean ± SD), which is 15 fold lower than that in, for example, temporal neocortex of AD patients (69.2 ± 39.8 DCP/mm^2) [62].

Since the FLIM analysis is performed on a cell-by-cell basis, the neurons previously imaged by FLIM were located again with the help of the XY coordinate system of the motorized stage, and the distance between each neuron and the nearest plaque edge was measured (Fig. 2a). Plotting $\%E_{FRET}$ against the distance to plaques revealed a significant negative correlation between the two parameters ($r = -0.4900$, $p<0.0001$), with higher $\%E_{FRET}$ values in neurons in close proximity to plaques (Fig. 2b). Average $\%E_{FRET}$ in neurons located >200 μm from plaques did not significantly differ from that in control individuals or FTLD patients (8.9 ± 2.1% vs 8.3 ± 2.3%) (Fig. 1a, Fig. 2b).

To quantify the relative percentage of neurons in "closed" and "open" conformations in the CA1 area of the sAD brain, we divided the data in arbitrary discrete intervals of 100 μm from the edge of a visible plaque in each brain section. Neurons with $\%E_{FRET}$ equal to ~8.96 ± 2.16%, corresponding to PS1 conformation in neurons farthest from the plaques (>200um, Fig.2b) and comparable to that in control human brain, were counted as neurons with an "open" PS1 conformation. All $\%E_{FRET}$ values above this threshold were considered as "closed" PS1 conformation. The contingency plot of the percent of neurons in "open" and "closed" conformations in each interval (Fig. 2c) shows a clear increase in the percentage of neurons with pathogenic "closed" PS1 conformation the closer they are to a plaque ($p<0.0001$, ^{2} –test for trend). This finding indicates that PS1 conformational changes are more profound in the vicinity of A plaques and suggests a link between PS1 conformation, amyloid deposition and the microenvironment surrounding Aβ plaques.

PS1 conformational changes are associated with aging

To further investigate the link between PS1 conformation, A deposition and aging, a longitudinal study in Tg2576 mice overexpressing SweAPP but having normal endogenous levels of wild-type PS1 was performed. Mice were divided into three age groups based on pathological and behavioral characteristics of the Tg2576 mouse model: **young animals (1–4 months)**, with no amyloid deposition and no behavioral anomalies; **adult animals (7–9 months)**, with no obvious amyloid deposition but gradual onset of memory impairment; and

old animals (17–25 months), with pronounced amyloid deposits and memory deficits [25,33,40].

PS1 conformation in the brain of young animals displayed a homogenous Gaussian distribution around a single mean value of $\%E_{FRET}$, corresponding to neurons with predominantly "open" PS1 conformation. At this young age, no difference between Tg2576 and non-transgenic littermates was observed (wt: 8.0 ± 2.2%; tg: 8.1 ± 2.1%) (Fig. 3a). In the adult mice group the average $\%E_{FRET}$ was also comparable between Tg2576 and non-transgenic littermates (Fig. 3b). However, whereas wild-type mice still showed a homogenous simple Gaussian distribution of the $\%E_{FRET}$ at values consistent with an "open" PS1 conformation (10.4 ± 1.5%), a small but significant subgroup of neurons with "closed" PS1 conformation was detected in adult Tg2576 animals. The distribution of PS1 conformation in these animals was found to follow a double Gaussian function with a first, larger peak corresponding to the values observed in non-transgenic animals i.e. "open" conformation (mean1 = 10.3 ± 2.3%), and a second, smaller peak with higher $\%E_{FRET}$ values indicating appearance of neurons that adopt a closed PS1 NT-CT conformation (mean2 = 17.5 ± 1.0%) (Fig. 3b). This second population of neurons was even more prominent in "old" Tg2576 animals, in which $\%E_{FRET}$ values followed a double Gaussian distribution with two equally weighted mean values (mean1 = 12.1 ± 2.7%, and mean2 = 20.9 ± 3.2%, respectively) (Fig. 3c). Thus, with aging and the onset of amyloid pathology, the originally small subpopulation of neurons with "closed" PS1 conformation observed in adult Tg2576 mice increases and even outweighs the initially dominant group of neurons with "open" PS1 conformation.

Remarkably, in the "old" wild-type group, although the majority of $\%E_{FRET}$ values corresponded to an "open" PS1 conformation (mean1 = 9.3 ± 2.2%) (Fig. 3c), a small but statistically significant population of neurons with high $\%E_{FRET}$, representing PS1 molecules with "closed" configuration, was also detected (mean2 = 22.6 ± 1.8%). This supports the idea that normal aging involves changes in PS1 conformation that are similar to changes caused by genetic or pharmacological manipulations previously found in *in vitro* studies [28,4,42,61]. Indeed, by using the same immunohistochemistry-based FLIM assay, we confirmed that APP/PS1 mice, which express ex9 mutant PS1 (an fAD mutation), display higher $\%E_{FRET}$ values than the non-transgenic littermates even at one month of age, validating our previous *in vitro* results [4] (Supplementary Fig. 1).

Oxidative stress triggers PS1 conformational changes in vitro and alters A production

It is well established that oxidative stress is a common factor implicated in both aging and AD [43,16]. The accumulation of reactive oxygen species (ROS) has been detected in the microenvironment of amyloid plaques in the brain [18,49]. To directly test that ROS may modify PS1 conformation, we induced oxidative stress in primary neurons by treating cells with a cell-permeant thiol-reactive oxidant 4,4′-dithiodipyridine (DTDP), or with an aldehyde product of lipid peroxidation 4-hydroxynonenal (HNE), which has been shown to accumulate in the brain during normal aging and is associated with AD pathology [12,69,58]. First, the generation of ROS in cells treated with DTDP or HNE was confirmed in living neurons by using CellROX Deep Red reagent, a sensitive marker that becomes fluorescent upon oxidation. As expected, both DTDP and HNE treated neurons showed significantly higher CellROX fluorescent signal compared to the vehicle treatment (vehicle: 1.00 ± 0.03, DTDP: 1.46 ± 0.09, HNE: 1.62 ± 0.10) (Supplementary Fig.2). Then, PS1 conformation was assessed by FLIM in neurons (sister cultures) exposed to DTDP or HNE for 20 min using either immunocytochemistry for endogenous PS1, or transfection with GFP-PS1-RFP FRET reporter probe [68]. We found that treatment with oxidizing agents significantly increased average $\%E_{FRET}$, compared to that in vehicle-treated neurons

(vehicle: 6.0 ± 0.3%, DTDP: 9.8 ± 0.5%, HNE: 8.3 ± 0.4%), indicating increased proximity between fluorescently labeled domains of the PS1 molecule (Fig 4a). The pseudo-colored FLIM images of neurons show significant shortening of the donor fluorophore lifetimes (yellow-to-red pixels) reflecting PS1 molecules adopting "closed" conformational state in neurons treated with oxidizing agent (Fig. 4b).

To ensure that the observed PS1 conformational changes were specific to oxidative stress, neurons were pre-incubated overnight with 750 μM antioxidant reagent, N-acetylcysteine amide (NACA), before the addition of DTDP or HNE. Reduction of the CellROX fluorescent signal in neuronal cultures pretreated with NACA prior to DTDP or HNE exposure confirmed that NACA was effective at decreasing the amount of ROS present in these cells (NACA-DTDP: 0.95 ± 0.06%, NACA-HNE: 1.18 ± 0.04%) (Supplementary Fig. 2). Accordingly, as shown in Fig. 4, pretreatment with NACA, but not with vehicle control, prevented the increase in $\%E_{FRET}$ induced by DTDP and HNE (NACA-DTDP: 5.8 ± 0.3%, NACA-HNE: 6.5 ± 0.4%). NACA itself had no significant effect on PS1 conformation, displaying comparable $\%E_{FRET}$ values to vehicle-treated cells (5.1 ± 0.3%). Of note, in accordance with our previously reported data [22], the observed change in PS1 conformation due to oxidative stress did not significantly affect PS1 ability to migrate on a native gel, as no difference between treated and non-treated cells was observed by blue native PAGE separation (not shown).

To assess whether the ROS-triggered changes in PS1 conformation directly translate into changes in A production, we measured A levels in the conditioned media after 3 hour treatment with DTDP or HNE. Remarkably, in such relatively short time after the treatment both oxidizing agents significantly increased the A 42/40 ratio, compared to that in vehicle treated cells (Fig. 5a). However, we observed a distinct effect of DTDP and HNE on the A production, with DTDP significantly decreasing A 40 and HNE significantly increasing A 42 generation (Fig.5 b,c). We have not observed any toxic effect of the drugs at the concentrations used, as determined by ToxiLight (Supplementary Fig.2c), indicating that variances in cell viability did not account for the observed changes in A production. These results strongly support the hypothesis that oxidative stress may locally increase the A 42/40 ratio by altering conformation of PS1/-secretase.

DISCUSSION

Over the past decades, a number of studies have helped to unravel the role of the AD-related gene PS1 in -secretase cleavage of APP and the subsequent release of A peptides of different lengths [reviewed in 14,60]. Familial AD mutations in PS1 are associated with increased production of longer highly fibrillogenic and neurotoxic A 42 species and, hence, increase the A 42/40 ratio [59,5,50].

We have previously established a PS1 conformation sensitive FLIM assay that monitors relative proximity between the fluorescently labeled PS1 N-and C-termini in intact cells with high spatial resolution. Using this assay we have shown that fAD PS1 mutations that increase the A 42/40 ratio consistently shift PS1 into a close PS1 NT-CT proximity conformation (we termed it "closed" PS1 conformation) in cells *in vitro* [4].

In the present study we applied this assay to tissue, and observed that endogenous wild type PS1 also adopts pathogenic "closed" conformation in CA1 hippocampal pyramidal neurons in sporadic AD brain, a change similar to that observed in cells bearing familial AD PS1 mutations [4] and in mice expressing fAD mutation ex9 PS1 (Supplementary Fig.1). We propose that changes in PS1 conformation are associated with AD/amyloid pathology: "closed" PS1 conformation was predominantly found in the vicinity of amyloid plaques in

AD patients, whereas in the brains of patients with FTLD, another neurodegenerative disorder without amyloid deposits [34], PS1 conformation did not significantly differ from that of non-demented controls. The diseased (AD and FTLD) and control brain tissue samples were of comparable postmortem intervals, and were obtained and processed in a similar manner, thus it is unlikely that the observed difference in PS1 conformation is due to any artifacts introduced during experimental manipulation. Moreover, different neurons within the same section of AD brain had PS1 in different conformational states; further validating specificity and sensitivity of the FLIM assay to detect variations in PS1 conformation. Thus, the finding that PS1 conformational shift is not a general result of neurodegeneration but rather is specifically associated with A pathology implies a strong link between structural changes in PS1 and A deposition.

Clinical-pathological and A PET imaging studies have convincingly shown that plaque deposition precedes cognitive decline, suggesting that accumulation of toxic A species may trigger a cascade of events in the aging brain, that may ultimately lead to sAD [27,29]. However, molecular alterations upstream of the toxic A species generation in the aged brain have not been fully elucidated. We propose that PS1 conformational changes that are associated with shifting -cleavage site on APP towards longer A species occur during normal aging and lead to A deposition in the brain. To establish this correlation we have characterized the timeline of A plaques formation and PS1 changes in the mouse brain. Our findings indicate that while young pre-plaque Tg2576 mice show a uniform distribution of the $\%E_{FRET}$ (neurons with predominantly “open” PS1 conformation), adult Tg2576 mouse brain contains a small subgroup of neurons with predominantly “closed” pathogenic conformation, even before the onset of amyloid deposition. Of note, previous reports have shown that at this age oligomeric A species can already be detected in the Tg2576 mouse brain and first behavioral symptoms appear [25,40]. Interestingly, the longitudinal study of non-transgenic littermate mice revealed the appearance of a small subpopulation of neurons with PS1 in the “closed” conformational state in the old group (17–25 months of age). A similar pattern of bimodal distribution was observed in human CA1 hippocampal neurons from aged control individuals, providing further evidence that PS1 conformational changes occur during normal aging and that these are upstream of the amyloid deposition. This is the first time that pathogenic conformation has been detected in wild-type PS1 during normal aging in non-demented individuals (as well as in sporadic AD); a finding that could be crucial for future therapeutic strategies focusing on allosteric -secretase modulators.

It should be noted that Tg2576 mice overexpress an fAD mutant APP (SweAPP), and produce high levels of A which in turn might induce pathologic alterations in the brain (e.g., generate ROS). Thus, it cannot be completely ruled out that pathogenic change in PS1 in these mice could be the *consequence* and not the *cause* of amyloid deposition. However, since we also observe appearance of PS1 in “closed” conformation in old wild type mice expressing physiological levels of endogenous APP, we do not believe that APP overexpression *per se* is linked to this pathogenic change. Moreover, our *in vitro* experiments directly show that “closed” PS1 conformation and elevated A 42/40 ratio are triggered by relatively short exposure to ROS, supporting the hypothesis that pathogenic conformational changes of PS1/-secretase might prompt local amyloid plaque formation over time. The appearance of PS1 in “closed” conformation, however, is observed much earlier in Tg2576 mice, as compared to non-transgenic littermates, supporting the existence of a positive feed-forward loop (see model in Fig.6).

It is conceivable that age-related stress factors in normal brain may trigger PS1 conformational changes in a subpopulation of neurons, resulting in a locally increased A 42/40 ratio, that in turn promotes toxicity and A deposition, which feeds into a vicious circle of events and ultimately leads to neurodegeneration (Fig. 6). Whether these more susceptible

(or more resistant) pyramidal neurons within the CA1 area of hippocampus belong to a different subtype of neurons or have different phenotypic characteristics is not known, and should be examined more closely in future studies.

Growing evidence supports the hypothesis that the most profound synaptic failure and dendritic spine loss occurs in the immediate vicinity to Aβ plaques [35,45]. Precise toxic factors near amyloid plaques have not been fully elucidated, however several markers of inflammation, oxidative stress, calcium dysregulation, and a halo of soluble oligomeric A species surrounding plaques have been reported [36,65,35,8,49,18]. Concurrent with this data, we demonstrate that "closed" PS1 conformation is predominantly found in close proximity to A deposits in the hippocampus of sporadic AD patients.

On the other hand, reactive oxygen species (ROS) are known to accumulate in the human brain as a result of normal aging (reviewed in [16]) and have been implicated in many neurodegenerative diseases, including AD [10,18,63,49,12]. Increase in ROS may derive from multiple sources, including astrocytes and microglia, A itself, and/or may be due to an impairment of the antioxidant defenses. Moreover, markers of oxidative stress have been detected prior to A deposition in a mouse model of AD [53]. Following this idea, we tested the hypothesis that ROS may be one of the triggering stress factors altering conformation of PS1/-secretase, thus leading to a local change in the A 42/40 ratio. Indeed, our recently published data show that peroxinitrite, an oxidant that accumulates during aging, induces PS1 conformational changes in cells *in vitro*, resulting in changes in the Aβ 42/40 ratio [22]. Here we demonstrate that this pathogenic outcome is not limited to a nitrosative stress, and different type of oxidants, such as the product of lipid peroxidation HNE and the thiol-reactive DTDP, significantly alter the Aβ 42/40 ratio by inducing pathogenic conformation of PS1/-secretase. Interestingly, recent data by Gwon et al. indicate that HNE can directly modify Nicastrin, one of the -secretase components. This modification results in increased -secretase activity and elevated A 42/40 ratio, thus promoting A deposition [23].

The idea that an aberrantly oxidized enzyme could mimic its mutant disease-linked version has also been proposed for amyotrophic lateral sclerosis (ALS). Cu/Zn superoxide dismutase (SOD1) in sporadic ALS has been reported to share the aberrant conformation characteristic of familial ALS-linked SOD1 mutant due to its abnormal oxidation. This suggests a common mechanism of toxicity between both forms of the disease [6,21]. We propose that a similar process is happening with PS1 in AD (familial vs. sporadic).

In spite of the wealth of evidence linking oxidative stress and AD, anti-oxidant therapies have so far failed to improve cognition in clinical trials [56,9,17]. It is worth mentioning, though, that all these clinical trials targeted patients with mild- to moderate probable AD, who according to the new clinical diagnostic criteria, are already in the amyloid-independent stage of the disease [26,48]. These failures emphasize the need to understand early events that precede the onset of symptoms, and to find therapeutic targets at these early stages. Our study proposes a possible mechanism of A 42/40 ratio deregulation and A deposition during aging, which could be useful in the development of therapeutic strategies designed to allosterically "correct" abnormal conformation of PS1/-secretase (as opposed to inhibit its function) before A accumulates in the brain.

Supplementary Material

Refer to Web version on PubMed Central for supplementary material.

Acknowledgments

We thank Dr. Bradley T. Hyman, Dr. Matthew Frosch, Karlotta Fitch, and the Alzheimer's Disease Research Centre for providing the human brain tissue that was used in this study. This work was supported by National Institutes of Health Grant [AG15379 to O.B.]; the German National Academic Foundation ("Studienstiftung des deutschen Volkes") [scholarship to L.W.]; the Fundacion Ibercaja (Zaragoza, Spain) [fellowship to M.A.]; the Fundacion Alfonso Martin Escudero (Madrid, Spain) [fellowship to A.S.P.].

References

1. Annaert WG, Esselens C, Baert V, et al. Interaction with telencephalin and the amyloid precursor protein predicts a ring structure for presenilins. Neuron. 2001; 32(4):579–589. [PubMed: 11719200]
2. Arriagada PV, Marzloff K, Hyman BT. Distribution of Alzheimer-type pathologic changes in nondemented elderly individuals matches the pattern in Alzheimer's disease. Neurology. 1992; 42(9):1681–1688. [PubMed: 1307688]
3. Berezovska O, Frosch M, McLean P, et al. The Alzheimer-related gene presenilin 1 facilitates notch 1 in primary mammalian neurons. Brain Res Mol Brain Res. 1999; 69(2):273–280. [PubMed: 10366748]
4. Berezovska O, Lleo A, Herl LD, et al. Familial Alzheimer's disease presenilin 1 mutations cause alterations in the conformation of presenilin and interactions with amyloid precursor protein. J Neurosci. 2005; 25(11):3009–3017. [PubMed: 15772361]
5. Borchelt DR, Thinakaran G, Eckman CB, et al. Familial Alzheimer's disease-linked presenilin 1 variants elevate Abeta1–42/1–40 ratio in vitro and in vivo. Neuron. 1996; 17(5):1005–1013. [PubMed: 8938131]
6. Bosco DA, Morfini G, Karabacak NM, et al. Wild-type and mutant SOD1 share an aberrant conformation and a common pathogenic pathway in ALS. Nature Neurosci. 2010; 13(11):1396–1403. [PubMed: 20953194]
7. Braak H, Braak E. Neuropathological stageing of Alzheimer-related changes. Acta Neuropath. 1991; 82(4):239–259. [PubMed: 1759558]
8. Brown GC, Bal-Price A. Inflammatory neurodegeneration mediated by nitric oxide, glutamate, and mitochondria. Mol Neurobiol. 2003; 27(3):325–355. [PubMed: 12845153]
9. Burke WJ, Roccaforte WH, Wengel SP, et al. L-deprenyl in the treatment of mild dementia of the Alzheimer type: results of a 15-month trial. Journal of the American Geriatrics Society. 1993; 41(11):1219–1225. [PubMed: 8227897]
10. Butterfield DA, Reed T, Sultana R. Roles of 3-nitrotyrosine- and 4-hydroxynonenal-modified brain proteins in the progression and pathogenesis of Alzheimer's disease. Free Radical Res. 2011; 45(1):59–72. [PubMed: 20942567]
11. Citron M, Westaway D, Xia W, et al. Mutant presenilins of Alzheimer's disease increase production of 42-residue amyloid beta-protein in both transfected cells and transgenic mice. Nature Med. 1997; 3(1):67–72. [PubMed: 8986743]
12. Cutler RG, Kelly J, Storie K, et al. Involvement of oxidative stress-induced abnormalities in ceramide and cholesterol metabolism in brain aging and Alzheimer's disease. Proc Natl Acad Sci U S A. 2004; 101(7):2070–2075. [PubMed: 14970312]
13. De Strooper B, Saftig P, Craessaerts K, et al. Deficiency of presenilin-1 inhibits the normal cleavage of amyloid precursor protein. Nature. 1998; 391(6665):387–390. [PubMed: 9450754]
14. De Strooper B, Vassar R, Golde T. The secretases: enzymes with therapeutic potential in Alzheimer disease. Nat Rev Neurol. 2010; 6(2):99–107. [PubMed: 20139999]
15. DeKosky ST, Scheff SW. Synapse loss in frontal cortex biopsies in Alzheimer's disease: correlation with cognitive severity. Ann Neurol. 1990; 27(5):457–464. [PubMed: 2360787]
16. Finkel T, Holbrook NJ. Oxidants, oxidative stress and the biology of ageing. Nature. 2000; 408(6809):239–247. [PubMed: 11089981]
17. Galasko DR, Peskind E, Clark CM, et al. Antioxidants for Alzheimer Disease: A Randomized Clinical Trial With Cerebrospinal Fluid Biomarker Measures. Archives Neurol. 201210.1001/archneurol.2012.85

18. Garcia-Alloza M, Dodwell SA, Meyer-Luehmann M, et al. Plaque-derived oxidative stress mediates distorted neurite trajectories in the Alzheimer mouse model. Journal of neuropathology and experimental neurology. 2006; 65(11):1082–1089. [PubMed: 17086105]
19. Gomez-Isla T, Hollister R, West H, Mui S, Growdon JH, Petersen RC, Parisi JE, Hyman BT. Neuronal loss correlates with but exceeds neurofibrillary tangles in Alzheimer's disease. J Neuropathol Exp Neurol. 1997; 65(11):1082–9.
20. Gomez-Isla T, Price JL, McKeel DW, et al. Profound loss of layer II entorhinal cortex neurons occurs in very mild Alzheimer's disease. J Neurosci. 1996; 16(14):4491–4500. [PubMed: 8699259]
21. Guareschi S, Cova E, Cereda C, et al. An over-oxidized form of superoxide dismutase found in sporadic amyotrophic lateral sclerosis with bulbar onset shares a toxic mechanism with mutant SOD1. Proc Natl Acad Sci U S A. 2012; 109(13):5074–5079. [PubMed: 22416121]
22. Guix FX, Wahle T, Vennekens K, et al. Modification of gamma-secretase by nitrosative stress links neuronal aging to sporadic alzheimer's disease. EMBO Mol Med. 2012; 4(7):660–673. [PubMed: 22488900]
23. Gwon AR, Park JS, Arumugam TV, et al. Oxidative lipid modification of nicastrin enhances amyloidogenic gamma-secretase activity in Alzheimer's disease. Aging cell. 2012
24. Hardy J, Selkoe DJ. The amyloid hypothesis of Alzheimer's disease: progress and problems on the road to therapeutics. Aging Cell. 2002; 11(4):559–568.
25. Hsiao K, Chapman P, Nilsen S, et al. Correlative memory deficits, Abeta elevation, and amyloid plaques in transgenic mice. Science. 1996; 274(5284):99–102. [PubMed: 8810256]
26. Hyman BT. Amyloid-dependent and amyloid-independent stages of Alzheimer disease. Arch Neurol. 2011; 68(8):1062–1064. [PubMed: 21482918]
27. Ingelsson M, Fukumoto H, Newell KL, et al. Early Abeta accumulation and progressive synaptic loss, gliosis, and tangle formation in AD brain. Neurology. 2004; 62(6):925–931. [PubMed: 15037694]
28. Isoo N, Sato C, Miyashita H, et al. Abeta42 overproduction associated with structural changes in the catalytic pore of gamma-secretase: common effects of Pen-2 N-terminal elongation and fenofibrate. J Biol Chem. 2007; 282(17):12388–12396. [PubMed: 17329245]
29. Jack CR Jr, Lowe VJ, Weigand SD, et al. Serial PIB and MRI in normal, mild cognitive impairment and Alzheimer's disease: implications for sequence of pathological events in Alzheimer's disease. Brain. 2009; 132(Pt 5):1355–1365. [PubMed: 19339253]
30. Jones PB, Rozkalne A, Meyer-Luehmann M, et al. Two postprocessing techniques for the elimination of background autofluorescence for fluorescence lifetime imaging microscopy. J Biomed Opt. 2008; 13(1):014008. [PubMed: 18315366]
31. Josephs KA. Frontotemporal dementia and related disorders: deciphering the enigma. Ann Neurol. 2008; 64(1):4–14. [PubMed: 18668533]
32. Kakuda N, Akazawa K, Hatsuta H, et al. Suspected limited efficacy of gamma-secretase modulators. Neurobiol Aging. 201210.1016/j.neurobiolaging.2012.08.017
33. Kawarabayashi T, Younkin LH, Saido TC, et al. Age-dependent changes in brain, CSF, and plasma amyloid (beta) protein in the Tg2576 transgenic mouse model of Alzheimer's disease. J Neurosci. 2001; 21(2):372–381. [PubMed: 11160418]
34. Kertesz A, McMonagle P, Blair M, et al. The evolution and pathology of frontotemporal dementia. Brain. 2005; 128(Pt 9):1996–2005. [PubMed: 16033782]
35. Koffie RM, Meyer-Luehmann M, Hashimoto T, et al. Oligomeric amyloid beta associates with postsynaptic densities and correlates with excitatory synapse loss near senile plaques. Proc Natl Acad Sci U S A. 2009; 106(10):4012–4017. [PubMed: 19228947]
36. Kuchibhotla KV, Goldman ST, Lattarulo CR, et al. Abeta plaques lead to aberrant regulation of calcium homeostasis in vivo resulting in structural and functional disruption of neuronal networks. Neuron. 2008; 59(2):214–225. [PubMed: 18667150]
37. Kuperstein I, Broersen K, Benilova I, et al. Neurotoxicity of Alzheimer's disease Abeta peptides is induced by small changes in the Abeta42 to Abeta40 ratio. EMBO J. 2010; 29(19):3408–3420. [PubMed: 20818335]

38. Lakowicz JR. Principles of frequency-domain fluorescence spectroscopy and applications to cell membranes. Sub-cellular Biochem. 1988; 13:89–126.
39. Lakowicz JR, Szmacinski H, Nowaczyk K, et al. Fluorescence lifetime imaging. Anal Biochem. 1992; 202(2):316–330. [PubMed: 1519759]
40. Lesne S, Koh MT, Kotilinek L, et al. A specific amyloid-beta protein assembly in the brain impairs memory. Nature. 2006; 440(7082):352–357. [PubMed: 16541076]
41. Lewczuk P, Esselmann H, Otto M, et al. Neurochemical diagnosis of Alzheimer's dementia by CSF Abeta42, Abeta42/Abeta40 ratio and total tau. Neurobiol Aging. 2004; 25(3):273–281. [PubMed: 15123331]
42. Lleo A, Berezovska O, Herl L, et al. Nonsteroidal anti-inflammatory drugs lower Abeta42 and change presenilin 1 conformation. Nature Med. 2004; 10(10):1065–1066. [PubMed: 15448688]
43. Lovell MA, Markesbery WR. Oxidative damage in mild cognitive impairment and early Alzheimer's disease. J Neurosci Res. 2007; 85(14):3036–3040. [PubMed: 17510979]
44. Mackenzie IR, Neumann M, Bigio EH, et al. Nomenclature and nosology for neuropathologic subtypes of frontotemporal lobar degeneration: an update. Acta Neuropath. 2010; 119(1):1–4. [PubMed: 19924424]
45. Masliah E, Mallory M, Hansen L, et al. Quantitative synaptic alterations in the human neocortex during normal aging. Neurology. 1993; 43(1):192–197. [PubMed: 8423884]
46. McKhann G, Drachman D, Folstein M, et al. Clinical diagnosis of Alzheimer's disease: report of the NINCDS-ADRDA Work Group under the auspices of Department of Health and Human Services Task Force on Alzheimer's Disease. Neurology. 1984; 34(7):939–944. [PubMed: 6610841]
47. McKhann GM, Albert MS, Grossman M, et al. Clinical and pathological diagnosis of frontotemporal dementia: report of the Work Group on Frontotemporal Dementia and Pick's Disease. Archives Neurol. 2001; 58(11):1803–1809.
48. McKhann GM, Knopman DS, Chertkow H, et al. The diagnosis of dementia due to Alzheimer's disease: recommendations from the National Institute on Aging-Alzheimer's Association workgroups on diagnostic guidelines for Alzheimer's disease. Alzheimer's & Dementia. 2011; 7(3):263–269.
49. McLellan ME, Kajdasz ST, Hyman BT, Bacskai BJ. In vivo imaging of reactive oxygen species specifically associated with thioflavine S-positive amyloid plaques by multiphoton microscopy. J Neurosci. 2003; 23(6):2212–2217. [PubMed: 12657680]
50. Morishima-Kawashima M, Ihara Y. Alzheimer's disease: beta-Amyloid protein and tau. J Neurosci Res. 2002; 70(3):392–401. [PubMed: 12391602]
51. NIA-RI. Consensus recommendations for the postmortem diagnosis of Alzheimer's disease. The National Institute on Aging, and Reagan Institute Working Group on Diagnostic Criteria for the Neuropathological Assessment of Alzheimer's Disease. Neurobiol Aging. 1997; 18(4 Suppl):S1–2. [PubMed: 9330978]
52. Placanica L, Zhu L, Li YM. Gender- and age-dependent gamma-secretase activity in mouse brain and its implication in sporadic Alzheimer disease. PLoS One. 2009; 4(4):e5088. [PubMed: 19352431]
53. Pratico D, Uryu K, Leight S, et al. Increased lipid peroxidation precedes amyloid plaque formation in an animal model of Alzheimer amyloidosis. J Neurosci. 2001; 21(12):4183–4187. [PubMed: 11404403]
54. Rodrigue KM, Kennedy KM, Park DC. Beta-amyloid deposition and the aging brain. Neuropsychol Rev. 2009; 19(4):436–450. [PubMed: 19908146]
55. Saito T, Suemoto T, Brouwers N, et al. Potent amyloidogenicity and pathogenicity of Abeta43. Nat Neurosci. 2011; 14(8):1023–1032. [PubMed: 21725313]
56. Sano M, Ernesto C, Thomas RG, et al. A controlled trial of selegiline, alpha-tocopherol, or both as treatment for Alzheimer's disease. The Alzheimer's Disease Cooperative Study. NE J Med. 1997; 336(17):1216–1222.
57. Savonenko A, Xu GM, Melnikova T, et al. Episodic-like memory deficits in the APPswe/PS1dE9 mouse model of Alzheimer's disease: relationships to beta-amyloid deposition and neurotransmitter abnormalities. Neurobiol Dis. 2005; 18(3):602–617. [PubMed: 15755686]

58. Sayre LM, Zelasko DA, Harris PL, et al. 4-Hydroxynonenal-derived advanced lipid peroxidation end products are increased in Alzheimer's disease. J Neurochem. 1997; 68(5):2092–2097. [PubMed: 9109537]
59. Scheuner D, Eckman C, Jensen M, et al. Secreted amyloid beta-protein similar to that in the senile plaques of Alzheimer's disease is increased in vivo by the presenilin 1 and 2 and APP mutations linked to familial Alzheimer's disease. Nature Med. 1996; 2(8):864–870. [PubMed: 8705854]
60. Selkoe DJ. Alzheimer's disease: genes, proteins, and therapy. Physiol Rev. 2001; 81(2):741–766. [PubMed: 11274343]
61. Serneels L, Van Biervliet J, Craessaerts K, et al. gamma-Secretase heterogeneity in the Aph1 subunit: relevance for Alzheimer's disease. Science. 2009; 324(5927):639–642. [PubMed: 19299585]
62. Serrano-Pozo A, Mielke ML, Gomez-Isla T, et al. Reactive glia not only associates with plaques but also parallels tangles in Alzheimer's disease. Amer J Pathol. 2011; 179(3):1373–1384. [PubMed: 21777559]
63. Sultana R, Butterfield DA. Role of oxidative stress in the progression of Alzheimer's disease. J Alzheimer's Dis: JAD. 2010; 19(1):341–353.
64. Terry RD, Masliah E, Salmon DP, et al. Physical basis of cognitive alterations in Alzheimer's disease: synapse loss is the major correlate of cognitive impairment. Ann Neurol. 1991; 30(4): 572–580. [PubMed: 1789684]
65. Texido L, Martin-Satue M, Alberdi E, et al. Amyloid beta peptide oligomers directly activate NMDA receptors. Cell Calcium. 2011; 49(3):184–190. [PubMed: 21349580]
66. Thinakaran G, Borchelt DR, Lee MK, et al. Endoproteolysis of presenilin 1 and accumulation of processed derivatives in vivo. Neuron. 1996; 17(1):181–190. [PubMed: 8755489]
67. Uemura K, Farner KC, Nasser-Ghodsi N, et al. Reciprocal relationship between APP positioning relative to the membrane and PS1 conformation. Mol Neurodegen. 2011; 6(1):15.
68. Uemura K, Lill CM, Li X, Peters JA, et al. Allosteric modulation of PS1/gamma-secretase conformation correlates with amyloid beta(42/40) ratio. PLoS One. 2009; 4(11):e7893. [PubMed: 19924286]
69. Williams TI, Lynn BC, Markesbery WR, Lovell MA. Increased levels of 4-hydroxynonenal and acrolein, neurotoxic markers of lipid peroxidation, in the brain in Mild Cognitive Impairment and early Alzheimer's disease. Neurobiol Aging. 2006; 27(8):1094–1099. [PubMed: 15993986]
70. Wiltfang J, Esselmann H, Bibl M, et al. Amyloid beta peptide ratio 42/40 but not A beta 42 correlates with phospho-Tau in patients with low- and high-CSF A beta 40 load. J Neurochem. 2007; 101(4):1053–1059. [PubMed: 17254013]
71. Wolfe MS. When loss is gain: reduced presenilin proteolytic function leads to increased Abeta42/Abeta40. Talking Point on the role of presenilin mutations in Alzheimer disease. EMBO reports. 2007; 8(2):136–140. [PubMed: 17268504]
72. Wolfe MS, Xia W, Ostaszewski BL, Diehl TS, et al. Two transmembrane aspartates in presenilin-1 required for presenilin endoproteolysis and gamma-secretase activity. Nature. 1999; 398(6727): 513–517. [PubMed: 10206644]
73. Yanagida K, Okochi M, Tagami S, et al. The 28-amino acid form of an APLP1-derived Abeta-like peptide is a surrogate marker for Abeta42 production in the central nervous system. EMBO Mol Med. 2009; 1(4):223–235. [PubMed: 20049724]

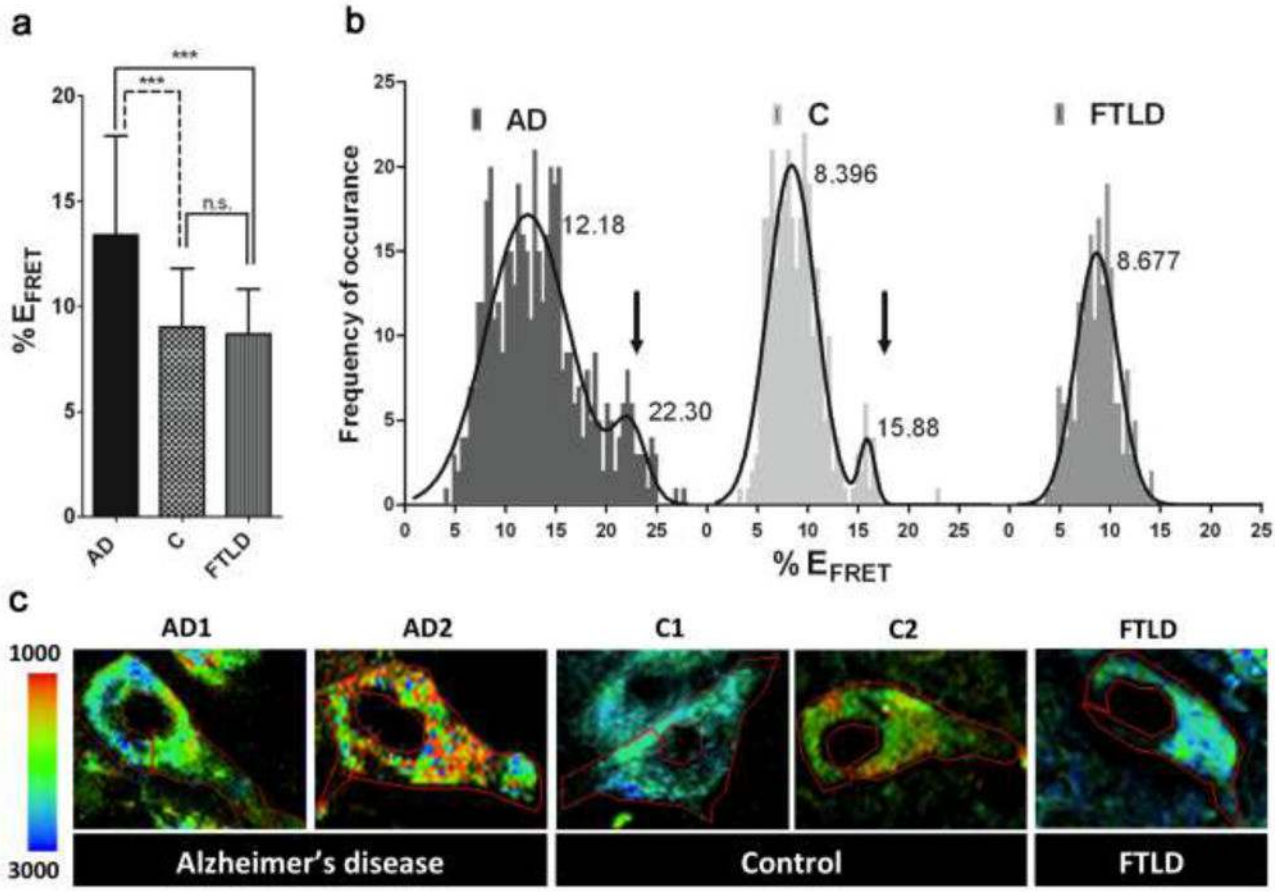

Figure 1. PS1 conformational changes occur in sporadic AD

FLIM analysis of different conformational states of PS1 molecules (%E_{FRET}) in CA1 hippocampal neurons in human brain. (a) Bar graph shows average %E_{FRET} and (b) histogram shows distribution of the %E_{FRET} values in sporadic AD (n = 10 cases, total of 477 neurons), non-demented control (n = 10 cases, total of 308 neurons) and FTLD (n = 5 cases, total of 196 neurons) brain tissue (mean ± SD; ***=p<0.001, n.s.= not significant; One-way ANOVA with Bonferroni's post-hoc correction (a), and Goodness-of-fit test with D'Agostino & Pearson omnibus normality test (b). Arrows in (b) show a subpopulation of neurons with "closed" PS1 conformation. (c) Color-coded FLIM images of representative neurons in CA1 area of AD, control, and FTLD brain samples. Donor fluorophore lifetimes in outlined cells represent different proximity between fluorophore-tagged domains on PS1 molecule, and thus PS1 in different conformations. Colorimetric scale shows fluorescence lifetime in picoseconds. Note: yellow-tored pixels represent PS1 molecules in "closed" conformation.

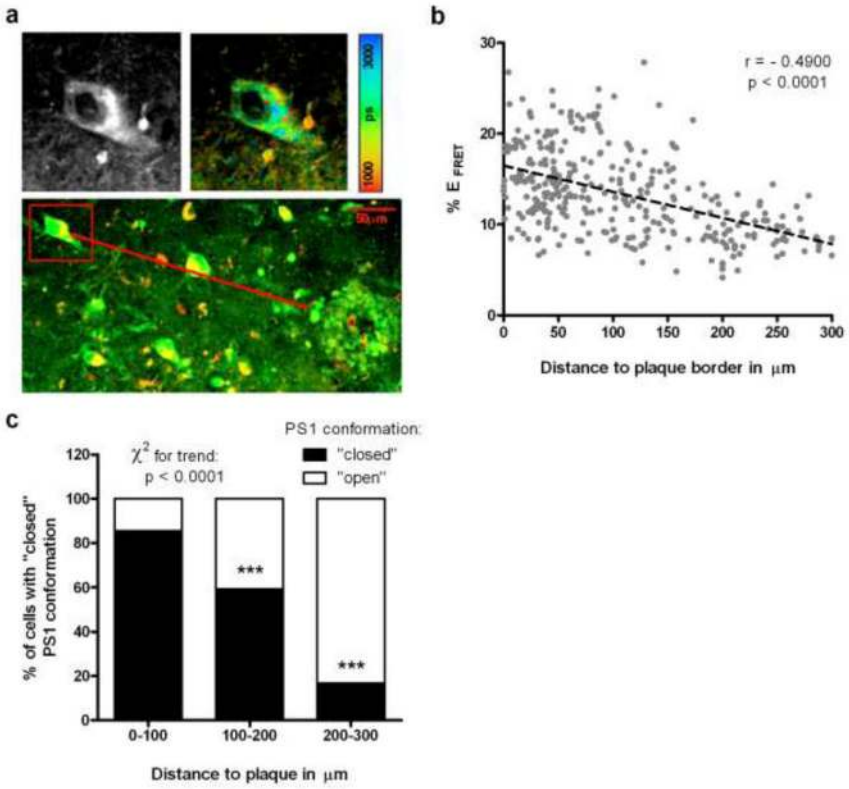

Figure 2. PS1 conformation correlates with proximity to ThioS positive A plaques

(a) Top panels show Alexa 488 fluorescence intensity image (left) and pseudo-colored FLIM image (right) of a neuron immunostained with Alexa488-labeled PS1 NT and Cy3-labeled PS1 CT antibodies. The pseudo-colored image displays donor fluorophore lifetimes calculated on a pixel-by-pixel basis, with red-to-yellow pixels representing shorter lifetimes. Colorimetric scale shows lifetime in picoseconds. The bottom panel shows a confocal fluorescence intensity image of the same neuron (red box) after ThioS counterstaining to determine its proximity to the A plaque. The distance between neurons and plaques was determined using Zeiss LSM510 software. (b) The scatter diagram shows distribution of the $\%E_{FRET}$ values in different neurons relative to their respective distance to the closest plaque (linReg: y=−0.02 X+15.9 with r= −0.49, p<0.0001). (c) The $\%E_{FRET}$ values from (b) were grouped and separated in 100 μm intervals to correlate the percent of neurons in “open” and “closed” conformations to A plaque proximity. (mean SD, ***=p<0.001, One way ANOVA).

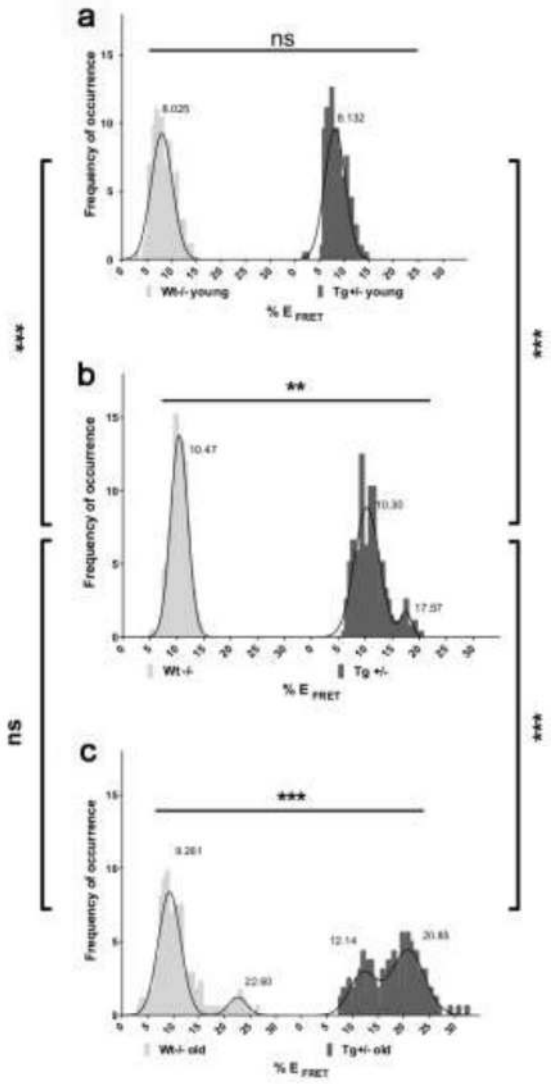

Figure 3. PS1 conformational changes are associated with aging

FLIM analysis in aging mouse brains reveals CA1 hippocampal neurons with different conformational states of the PS1 molecules. Histograms show distribution of the %E $_{FRET}$ values representing PS1 NT-CT proximity in neurons of Tg2576 (dark grey) and non-transgenic littermate (light grey) mice of different ages: (a) 2–4 months of age, young animals (wt: n = 172 neurons; tg: n = 198 neurons); (b) 7–9 months adult mice (wt: n = 217 neurons; tg: n = 273 neurons); and (c) >17 months of age, old animals (wt: n = 173 neurons; tg: n = 160 neurons) (mean SD; ***=p<0.001, **=p<0.01, ns= not significant; 2-sided student's t-test or One-way ANOVA with Bonferroni's post-hoc correction.)

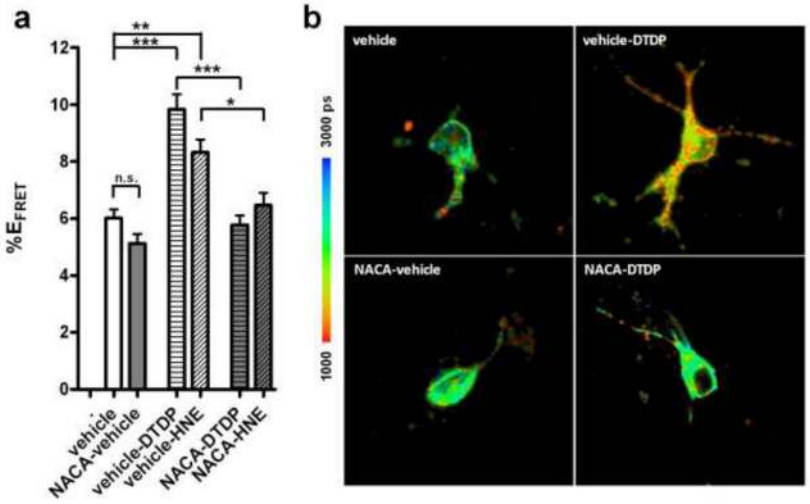

Figure 4. Oxidative stress triggers PS1 conformational changes in vitro

(a) Bar graph shows quantitative analysis of $\%E_{FRET}$ values in neurons treated with vehicle, NACA, DTDP, and/or HNE (vehicle: n = 167; NACA-vehicle: n = 216; vehicle-DTDP: n = 115, vehicle-HNE: n = 106; NACA-DTDP: n = 145; NACA-HNE: n = 125 neurons). The data are presented as mean ± SEM; (***p<0.001, **=p<0.01, *=p<0.05, n.s.= not significant; One-way ANOVA with Bonferroni's post-hoc correction). (b) Representative FLIM images of primary neurons transfected with GFP-PS1-RFP FRET reporter construct, and pretreated with NACA (or vehicle) before exposure to DTDP (or vehicle). The pseudo-colored images display donor fluorophore lifetimes, with yellow-to-red pixels representing PS1 in "closed" conformation. Colorimetric scale shows lifetime in picoseconds.

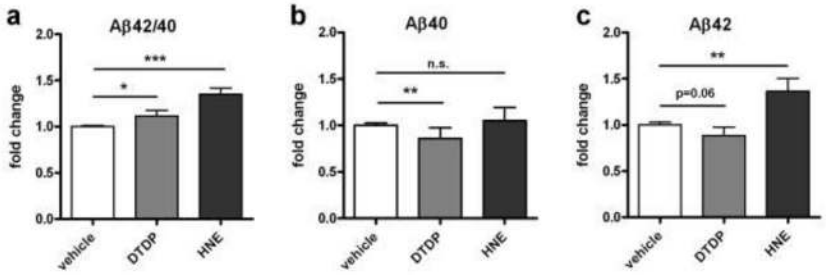

Figure 5. Effect of oxidative stress on A production

Primary neurons were treated with DTDP, HNE, or vehicle for 3 hours, and the condition media was collected to assess production of A 40 and A 42 by ELISA. The amount of each Aβ species is presented as fold-change after being normalized to that in the conditioned media of vehicle-treated control cells (vehicle: n = 10, DTDP: n = 11, HNE: n = 12 wells, three independent experiments). The data are shown as mean SEM (***p<0.001, **p<0.01, *p<0.05, ns= not significant; Mann Whitney non-parametric t-test).

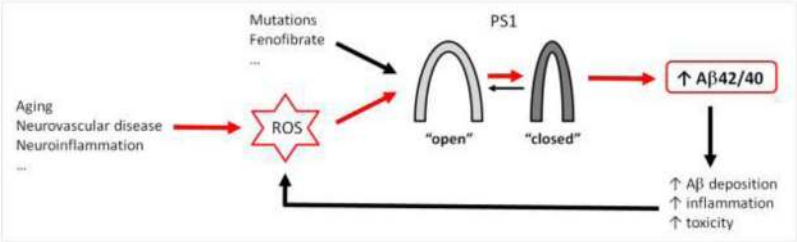

Figure 6.

Schematic representation of the hypothetical interplay between oxidative stress, PS1 conformational changes, and elevated A 42/40 ratio.

Elevated level of the oxidative stress (ROS) in the brain may induce local changes in the A 42/40 ratio and amyloidosis by altering conformation of PS1/-secretase. Accumulation of highly fibrillogenic A 42 species, subsequently, may cause oxidative stress, feeding into a positive, feed-forward cycle of deleterious events